Smart Mater. Struct. **20** (2011) 115001 (6pp) doi:10.1088/0964-1726/20/11/115001

Online monitoring of the distributed lateral displacement in large AC power generators using a high spatial resolution Brillouin optical fiber sensor

Yongkang Dong, Xiaoyi Bao and Liang Chen

Department of Physics, University of Ottawa, 150 Louis-Pasteur, Ottawa, ON, K1N 6N5, Canada

E-mail: aldendong@gmail.com, xbao@uottawa.ca and Liang.Chen@uottawa.ca

Received 2 June 2011, in final form 29 August 2011
Published 3 October 2011
Online at stacks.iop.org/SMS/20/115001

Abstract

We report for the first time, to the best of our knowledge, online monitoring of the distributed lateral displacement in large AC power generators using high spatial resolution differential pulse-width pair Brillouin optical time-domain analysis (DPP-BOTDA). To perform the measurement of distributed lateral displacements with periods of only a few cm in large AC power generators, a 2 cm spatial resolution strain measurement is realized using the differential pulse pair of 8/8.2 ns in DPP-BOTDA, and then the lateral displacements are reconstructed according to the strain–displacement relation with the assumption of a sine shape function. Using different fiberglass ripple springs, two types of lateral displacement with periods of 3 and 3.25 cm are demonstrated, obtaining a maximum displacement of 0.43 mm with a measurement accuracy of ~40 μm. This provides the information on the stator coil tightness through online monitoring of the distributed lateral displacement caused by the fiberglass ripple springs, and ensures safe operating conditions for large AC power generators. In addition, the large number of sensing points associated with distributed optical fiber sensors make it economically and technically practical to monitor large numbers of key components in a generator without any interference from the large magnetic and electrical fields.

(Some figures in this article are in colour only in the electronic version)

1. Introduction

The large AC power generators used in electric utility plants employ a large number of sensors to monitor different parameters, such as temperature, vibration, coolant flow, voltage, current, etc, to ensure safe operating conditions. However, even with such a large number of sensors in a generator, online failures still occur too often due to fatigue of the electrical insulation and mechanical components. Deterioration of the stator coil tightness may cause 'slot pounding', which has caused many generators to short to ground. During the installation of an AC power generator, the fiberglass ripple spring, which is located just below the stator wedge, must be sufficiently compressed to be flat or nearly flat to ensure the maximum tightness to compensate for the stator coil ground-wall insulation creep that is the primary factor in stator coil looseness resulting in 'slot pounding'. However, there is currently no reliable method for online monitoring of the condition of the stator coil tightness except during maintenance outages when the unit is disassembled and inspected by means of a robotic air-gap device, which performs a measurement of the lateral displacement of the flat plate under the ripple spring. For reasons of economics, the interval between two inspections is usually a few years, which leaves a lot of time for conditions to degrade without monitoring, thus real-time monitoring of the stator coil tightness is urgently needed to ensure safe operating conditions for a generator.

Because of their many advantages, such as immunity to electromagnetic interference, light weight, good flexibility, etc, optical fiber sensors are ideal candidates for online measurement in an environment with a high voltage and a high electromagnetic field in the generators. Usually, the fiberglass ripple springs used in the stator coil have a period of a few cm, which is a challenge in terms of the spatial resolution and the number of sensing points, so a high spatial resolution distributed sensing technique is preferred for such measurement. Brillouin optical fiber sensors have been successfully developed for distributed temperature and strain measurement over the past two decades [1–7]. Usually, the spatial resolution is limited to 1 m due to the phonon lifetime (∼10 ns in a silica fiber). Recently, a novel differential technique has been proposed in Brillouin optical time-domain analysis (BOTDA) using a pulse pair and a high spatial resolution can be achieved by using a small difference of the pulse pair [8, 9] based on the mechanism of pre-pumping the acoustic wave [10]. The differential pulse-width pair (DPP) technique in BOTDA is implemented as follows: first, two time traces of the Brillouin signal are obtained by using two pulses with different pulse-widths; second, the differential signal is obtained by making a subtraction between the two Brillouin signals, and then the differential Brillouin spectra can be obtained by sweeping the frequency offset in the vicinity of the Brillouin frequency shift (BFS). In the differential Brillouin spectra, the spatial resolution is determined by the differential pulse, i.e. the pulse-width difference of the pulse pair, rather than the original pulses.

In this paper, we demonstrate a measurement of the deformation caused by fiberglass ripple springs in large AC power generators using a high spatial resolution DPP-BOTDA. In the experiment, a sensing fiber is glued to a fiberglass flat plate, which is subjected to a periodic side force from a fiberglass ripple spring and is consequently characterized by a periodic deformation. First, a 2 cm spatial resolution is obtained by using the differential pulse pair of 8/8.2 ns in DPP-BOTDA, based on which the measurement of the longitudinal strain of the flat plate caused by the compression of the ripple spring is performed. Then the shape of the flat plate is reconstructed according to the strain–displacement relation with the assumption of a sine shape function. Measurements of distributed lateral displacement of the flat plate with different periods of 3 and 3.25 cm are demonstrated with a maximum displacement of 0.43 mm and a minimum measurable displacement of ∼40 μm.

2. Experimental setup and test-board layout

The experimental setup is shown in figure 1. Two narrow-linewidth fiber lasers operating at ∼1550 nm are used to provide the probe and pump waves of a BOTDA system, whose frequency difference is locked by a microwave frequency counter [11]. An electro-optic modulator with a high extinction ratio (ER > 40 dB) is used to generate the optical pulse, which is then amplified by an erbium-doped fiber amplifier before being launched into the sensing fiber. A piece of 2 m polarization maintaining (PM) fiber is used as the sensing fiber

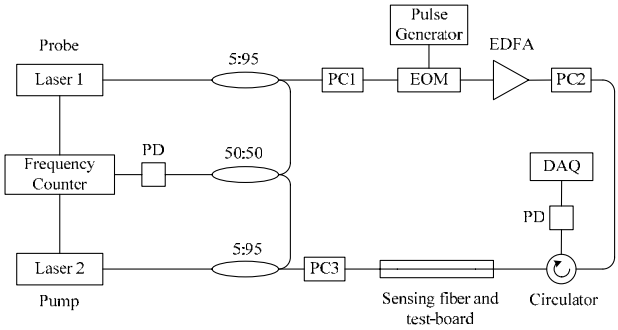

Figure 1. Experimental setup. PD: photo-detector, PC: polarization controller, EOM: electro-optic modulator, EDFA: erbium-doped fiber amplifier, DAQ: data acquisition.

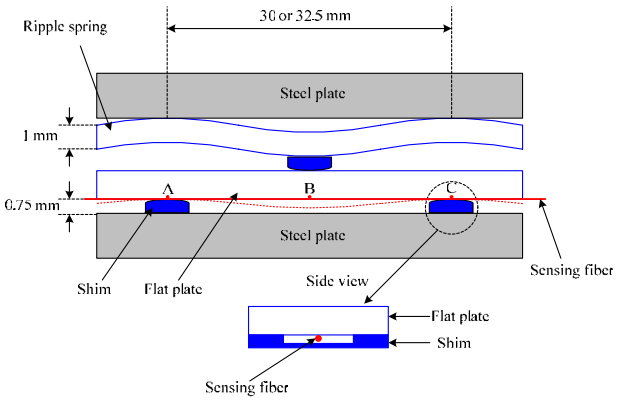

Figure 2. Schematic diagram of the test-board structure. The side view of the shim shows the sensing fiber and the groove in it.

to avoid polarization-dependent fluctuation, and its BFS is 10 600 MHz at 25 °C. Polarization controllers are used to align the pump and probe waves to one principal axis of the PM fiber. A 3.5 GHz bandwidth detector with a transition time (10%–90%) of 115 ps, which thus can resolve the cm-order variation in strain or temperature, is used to detect the Brillouin signal. The sampling rate of the digitizer is set at 40 GHz s^{-1}, which corresponds to 2.5 mm/point in the optical fiber.

Nominally, the spatial resolution of the differential Brillouin spectra in DPP-BOTDA is determined by the pulse-width difference of the pulse pair; however, the actual spatial resolution would be limited by the fall time of the pulse, which limits the applicable minimum duration of the differential pulse. In our experiment, a high-speed pulse generator is used to generate a square pulse with a fall time (90%–10%) of 150 ps, enabling a cm-order spatial resolution.

In order to provide an online measurement of stator coil tightness, the test-board configuration shown in figure 2 is tested and evaluated, where in an actual AC power generator the two steel plates are replaced by a high voltage stator coil and a stator wedge. Two steel plates sandwich a ripple spring with a sine profile and a flat plate. Small-size shims are placed under the spring valleys between the ripple spring and the flat plate and under the spring peaks between the flat plate and the bottom steel plate. One side of the shim contacting the flat plate is made to be an arc-shape. The ripple spring, flat

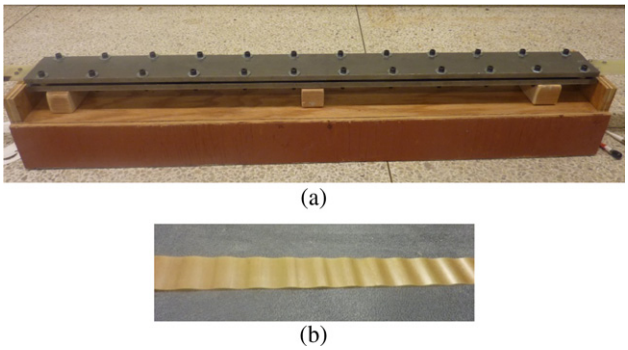

Figure 3. Photos of (a) the test-board and (b) the ripple spring.

plate and shims are all made of fiberglass, with thicknesses of 1 mm, 1 mm and 0.75 mm, respectively, and the widths of the ripple spring and flat plate are both 51 mm. In the experiment, two kinds of ripple spring with periods of 3 and 3.25 cm are tested; these two sizes are widely used by AC power generator manufactures.

When a side pressure is applied on the two steel plates, the ripple spring is subjected to a lateral extrusion force and is compressed to be flat or nearly flat, while the flat plate is compressed to form a new ripple spring because of the lateral extrusion force from the original ripple spring. In figure 2, the dotted red curve schematically shows the bottom surface profile of the flat plate after applying pressure. The sensing fiber is glued onto the bottom surface of the flat plate to measure the longitudinal strain, and it will not be subjected to the side pressure because of the groove in the shim, as shown in the side view of the shim in figure 2. Generally, the points under spring valleys such as point B will experience traction stress, while the points under spring peaks such as points A and C will initially see compression stress, which will cause longitudinal strains in the sensing fiber. It is noted that point B sees the maximum displacement, while the positions of points A and C remain unchanged.

Figure 3 shows photos of the test-board and the ripple spring used in this experiment. The two steel plates have the same size of 7.5 cm × 92 cm, and are fixed by 12 pairs of screws. Through fastening these screws, a side pressure can be applied on the ripple spring and the flat plate. Four pieces of ripple spring, including a long one with a length of 44 cm and a period of 3 cm and three short ones with a length of 15 cm and a period of 3.25 cm, are placed end-to-end on the test-board. After applying the side pressure, all of these ripple springs are compressed to be flat or nearly flat, while the flat plate turns into a longer continuous ripple spring.

3. Longitudinal strain measurement with DPP-BOTDA

In the DPP-BOTDA scheme, it is straightforward to understand that a higher spatial resolution can be obtained by shortening the pulse-width difference of the pulse pair. However, the differential signal suffers a reduction of signal-to-noise ratio (SNR) with respect to the original two signals, which will deteriorate the measured frequency accuracy. Therefore a tradeoff must be made to ensure a high spatial resolution with an adequate SNR. Previously, a 15 cm spatial resolution using a 20/19 ns pulse-width pair [9] and a 5 cm spatial resolution using a 30/29.5 π-phase-shift pulse pair were reported [13]. In our experiment, an 8/8.2 ns pulse pair is used to obtain an improved 2 cm spatial resolution.

The powers of the continuous wave and pulse wave of the BOTDA used in the experiment are set at 0.5 and 500 mW, respectively, and their frequency offset is scanned from 10 460 to 10 740 MHz with a step of 10 MHz. Each time trace of the Brillouin signal is averaged by a number of 2000 to reduce the noise. Figure 4 shows the top view of the measured three-dimensional differential Brillouin spectra by using a pulse pair of 8/8.2 ns. It is clearly seen that the ripple spring is in the region of 55–145 cm.

The fitted BFS and corresponding longitudinal strain are plotted in figure 5, where the BFS variation induced by the long ripple spring is denoted as region 1, and those induced by the other three short ones are denoted as regions 2, 3 and 4, respectively. Figure 5 clearly shows a periodic longitudinal strain along the sensing fiber, where the peaks and the valleys correspond to the positions under the spring valleys and peaks, respectively. Taking region 1 as an example, it is seen that the sensing fiber under the ripple spring is subjected to a

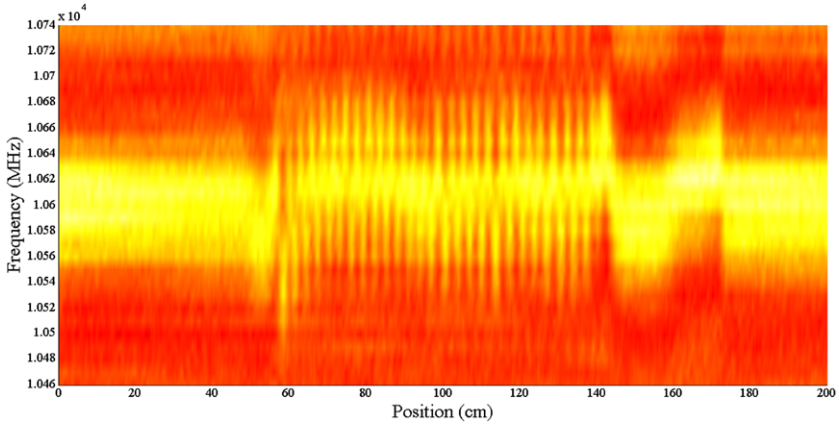

Figure 4. Top view of the measured three-dimensional differential Brillouin spectra with a pulse pair of 8/8.2 ns.

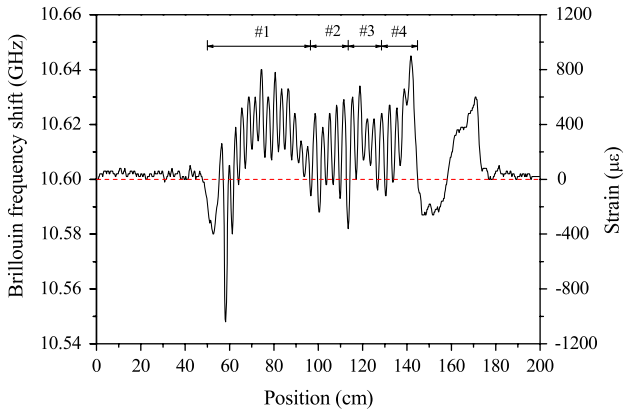

Figure 5. The fitted BFS and corresponding longitudinal strain as functions of position.

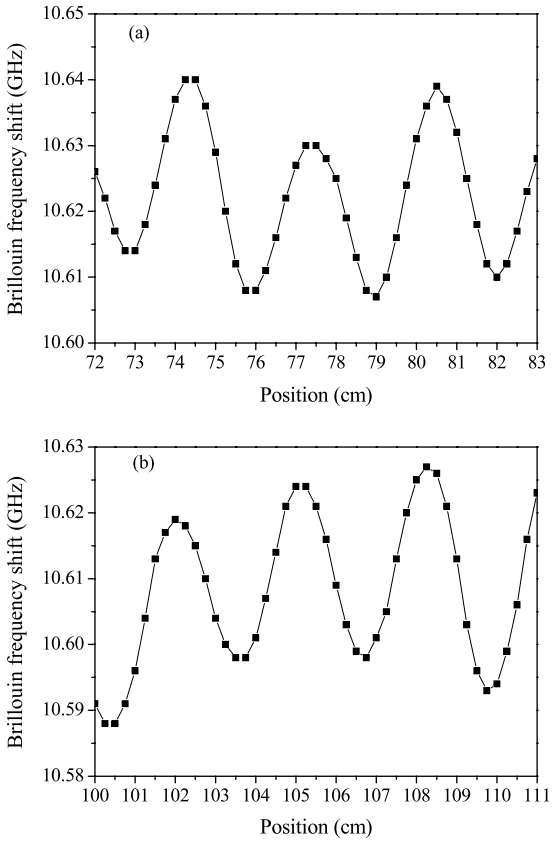

Figure 6. Enlarged partial BFS signal with different ripple spring periods of (a) 3 cm in region 1 and (b) 3.25 cm in region 2 in figure 5.

large positive longitudinal strain in the middle, and the value gradually decreases to negative toward its two ends, where a maximum negative strain of $-1040\ \mu\varepsilon$ is observed at the left end (the 58 cm position) of the long ripple spring. A similar trend can also be observed in the other three short ripple springs, which indicates that for individual springs the middle section always experiences a larger side pressure compared with the two end sections.

To show a detailed strain variation with different periods, the enlarged partial BFS signals of regions 1 and 2 in figure 5 are plotted in figure 6. Each point represents a 2.5 mm segment as a 40 GHz s^{-1} sampling rate is used. In figure 6(a), there are twelve points within one period, corresponding to the 3 cm period of the long ripple spring in region 1; figure 6(b) shows the 3.25 cm period of the short ripple spring in region 2.

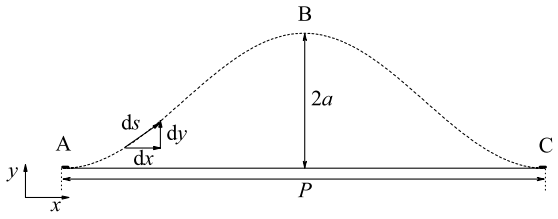

Figure 7. Shape profile with a sine function.

4. Lateral displacement reconstructions

The shape reconstruction, which derives displacement from strain data, has been extensively studied for different structures [12]. Since shape reconstruction is an inverse problem, the location of data points, number of data and data accuracy are important factors for obtaining accurate results. Compared with discrete sensing techniques, such as FBG sensors or strain gauges, a distributed sensing technique can provide a large number of strain values with cm or mm intervals, and thus accurate shape reconstruction can be performed.

As in the case shown in figure 2, the nodes under the spring peaks such as points A and C, which directly contact with the shims, stay still without lateral displacement; because of the small deformation, the shape profile between two nodes can be well assumed to be a sine function, as shown in figure 7.

We consider the curve of the displaced sensing fiber in three dimensions expressed as $[x, y(x), z(x)]$. For a differential section of the sensing fiber that is stretched from a length of $\mathrm{d}x$ to $\mathrm{d}s$ by the deformation, the longitudinal elongation $\mathrm{d}u$ is given by

$$\mathrm{d}u = \mathrm{d}s - \mathrm{d}x = \sqrt{1 + \left(\frac{\mathrm{d}y}{\mathrm{d}x}\right)^2 + \left(\frac{\mathrm{d}z}{\mathrm{d}x}\right)^2}\,\mathrm{d}x - \mathrm{d}x. \quad (1)$$

Omitting the displacement in the z direction, we have $\mathrm{d}z/\mathrm{d}x = 0$.

We assume that the shape function $y(x)$ describing the lateral displacements of the points along the sensing fiber from their initial positions follows a sine function, and is given by

$$y(x) = a \sin \frac{2\pi}{P} x \quad (2)$$

where P is the period and a is the amplitude, hence the lateral displacement of the middle point B is $2a$. Then the longitudinal elongation $\mathrm{d}u$ is given by

$$\mathrm{d}u = \sqrt{1 + \left(a\frac{2\pi}{P}\cos\frac{2\pi}{P}x\right)^2}\,\mathrm{d}x - \mathrm{d}x. \quad (3)$$

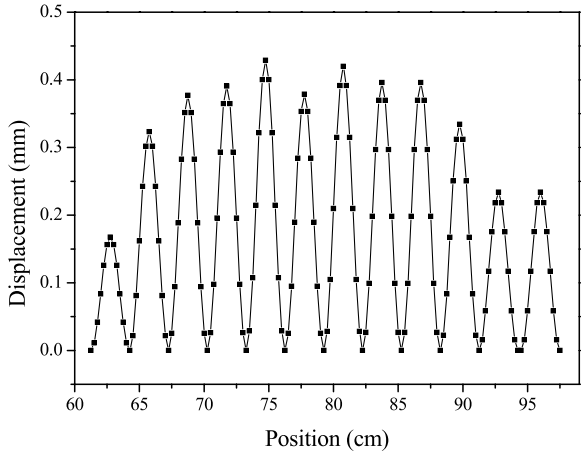

Figure 8. The lateral displacement reconstruction of the flat plate in region 1.

Under the condition of small deformation, i.e., $a = P$, we have $\left(a\frac{2\pi}{P}\cos\frac{2\pi}{P}x\right)^2 = 1$, then (3) can be expressed as

$$\mathrm{d}u \cong \frac{1}{2}\left(a\frac{2\pi}{P}\cos\frac{2\pi}{P}x\right)^2 \mathrm{d}x. \tag{4}$$

The elongation of the sensing fiber over a period can be obtained as

$$u \cong \int_0^P \frac{1}{2}\left(a\frac{2\pi}{P}\cos\frac{2\pi}{P}x\right)^2 \mathrm{d}x = \frac{a^2\pi^2}{P}. \tag{5}$$

Therefore the amplitude a can be expressed as

$$a = \frac{\sqrt{uP}}{\pi} = \frac{\sqrt{\int_0^P \varepsilon\,\mathrm{d}x\,P}}{\pi} \tag{6}$$

where ε is the longitudinal strain along the sensing fiber.

Omitting the first and last periods where the shape of the sensing fiber has a large deviation from the sine function, the lateral displacement reconstruction over the twelve periods in the middle of the long ripple spring in region 1 is plotted in figure 8. It is seen that the middle section sees larger displacement because of the higher side pressure than that of the two ends, while due to the nonuniform side pressure over a period the shape profile has a deviation from the sine function, which may cause a reconstruction error. A maximum displacement of 0.43 mm is observed at the position of 74.75 cm rather than the center of the ripple spring (position of 77.75 cm), whose lateral displacement is measured to be 0.37 mm.

The lateral displacement reconstruction error caused by the measured longitudinal strain accuracy can be given by

$$\delta a = \frac{\sqrt{\int_0^P \delta\varepsilon\,\mathrm{d}x\,P}}{\pi}. \tag{7}$$

The standard deviation of the measured BFS in figure 5 is calculated to be $\delta\nu_\mathrm{B} = 0.96$ MHz, which corresponds to a standard deviation of the longitudinal strain of $\delta\varepsilon = 19.9\ \mu\varepsilon$ according to the BFS strain coefficient of 0.0483 MHz/$\mu\varepsilon$ [4]. Therefore, for the spring periods of 3 and 3.25 cm, the minimum measurable displacements are calculated to be 41 and 45 μm, respectively. At the position of 65.75 cm, a hole is opened in the bottom steel plate to monitor the lateral displacement by a caliper, by which the measured lateral displacement is 0.35 mm with a deviation of 30 μm with respect to the reconstructed value of 0.32 mm from the measured longitudinal strain. There are a few sources to account for the displacement reconstruction error, such as the assumption of a sine function, nonuniform side pressure over a period and the measured longitudinal strain error. The above analysis shows that the real deviation is smaller than the calculated maximum measurement error through the standard deviation of the longitudinal strain, which indicates that the measured longitudinal strain error is the dominant origin for the lateral displacement reconstruction accuracy.

5. Discussion and conclusions

Note that the deformation of the flat plate originates from the ripple spring pressure, and a large pressure can maintain the stator coil tightness and avoid the stator coil 'slot pounding'. As the stator coil insulation ages and creeps, the ripple spring pressure decreases and the deflection curve of the flat plate will change until some points become loose resulting in 'slot pounding'. The longitudinal strain distribution of the flat plate directly reflects the deformation caused by the ripple spring pressure, showing the stator coil wedge tightness. The lateral displacement reconstruction of the flat plate according to the displacement–strain relation provides a clearer way to characterize the operating conditions of a generator.

To summarize, we have demonstrated online monitoring of the deformation caused by the fiberglass ripple springs in large AC power generators using a high spatial resolution DPP-BOTDA. Through optimizing the differential pulse pair of DPP-BOTDA, an improved 2 cm spatial resolution of the longitudinal strain measurement is realized by using the 8/8.2 ns pulse pair, which successfully resolves the deformations with periods of 3 and 3.25 cm caused by different ripple springs. The shape reconstruction of the flat plate shows a maximum lateral displacement of 0.43 mm and a minimum measurable displacement of ~40 μm.

Acknowledgments

This work was supported by the Natural Science and Engineering Research Council of Canada (NSERC) through a discovery and strategic grant and the Canada Research Chair Program. We also thank Mr George Dailey from Siemens Energy Inc. for providing the test-board.

References

[1] Horiguchi T, Kurashima T and Tateda M 1990 A technique to measure distributed strain in optical fibers *IEEE Photon. Technol. Lett.* **2** 352–4

[2] Bao X, Webb D J and Jackon D A 1993 22 km distributed temperature sensor using Brillouin gain in an optical fiber *Opt. Lett.* **18** 552–4

[3] Nikles M, Thevenaz L and Robert P A 1996 Simple distributed fiber sensor based on Brillouin gain spectrum analysis *Opt. Lett.* **21** 758–60
[4] Parker T R, Farhadiroushan M, Hankerek V A and Rogers A J 1997 Temperature and strain dependence of the power level and frequency of spontaneous Brillouin scattering in optical fibers *Opt. Lett.* **22** 787–9
[5] Maughan S M, Kee H H and Newson T P 2001 57 km single-ended spontaneous Brillouin-based distributed fiber temperature sensor using microwave coherent detection *Opt. Lett.* **26** 331–3
[6] Garus D, Gogolla T, Krebber K and Schliep F 1997 Brillouin optical-fiber frequency-domain analysis for distributed temperature and strain measurement *J. Lightwave Technol.* **15** 654–62
[7] Hotate K and Tanaka M 2002 Distributed fiber Brillouin strain sensing with 1 cm spatial resolution by correlation-based continuous-wave technique *IEEE Photon. Technol. Lett.* **14** 179–81
[8] Thevenaz L and Mafang S F 2008 Distributed fiber sensing using Brillouin echoes *Proc. SPIE* **7004** 70043N
[9] Li W, Bao X, Li Y and Chen L 2008 Differential pulse-width pair BOTDA for high spatial resolution sensing *Opt. Express* **16** 21616–25
[10] Bao X, Brown A, DeMerchant M and Smith J 1999 Characterization of the Brillouin gain/loss linewidth for single mode fibers using very short pulses *Opt. Lett.* **24** 510–2
[11] Dong Y, Bao X and Li W 2009 Differential Brillouin gain for improving the temperature accuracy and spatial resolution in a long-distance distributed fiber sensor *Appl. Opt.* **48** 4297–301
[12] Nishio M, Mizutani T and Takeda N 2010 Structural shape reconstruction with consideration of the reliability of distributed strain data from a Brillouin-scattering-based optical fiber sensor *Smart Mater. Struct.* **19** 035011
[13] Foaleng S M, Tur M, Beugnot J C and Thevenaz L 2010 High spatial and spectral resolution long-range sensing using Brillouin echoes *J. Lightwave Technol.* **28** 2993–3003